Results in Physics 57 (2024) 107368

Contents lists available at ScienceDirect

Results in Physics

journal homepage: www.elsevier.com/locate/rinp

Half-metallic ferromagnetic features of V-doped Cu_2O alloys: TB-mBJ and DFT + U insights

Mohammed El Amine Monir [a], Hadj Baltach [a], Ibtisam F. Al-Maaitah [b], A.F. Al-Maaitah [c], M.A. Ghebouli [d], M. Fatmi [d,*], Munirah D. Albaqami [e], Saikh Mohammad [e], Mourad Debbichi [f], Mika Sillanpää [g]

[a] Faculty of the Exact Sciences, Mustapha Stambouli University of Mascara, B.P. 305, 29000 Mascara, Algeria
[b] Applied Physics Department, Faculty of Science, Tafila Technical University, P.O. Box: 179, Tafila, Jordan
[c] Department of Physics, Mutah University, Mutah, Karak, 61710, P.O. Box: 7, Jordan
[d] Research Unit on Emerging Materials (RUEM), University Ferhat Abbas of Setif 1, Setif 19000, Algeria
[e] Department of Chemistry, College of Science, King Saud University, Riyadh 11451, Saudi Arabia
[f] Laboratoire de la Matière Condensée et Nanosciences LR11ES40, Faculté des Sciences de Monastir, Université de Monastir, 5019 Monastir, Tunisia
[g] Department of Biological and Chemical Engineering, Aarhus University, Norrebrogade 44, 8000 Aarhus C, Denmark

ARTICLE INFO

Keywords:
$Cu_{2(1-x)}V_{2x}O$ alloys
Structural properties
Electronic properties
Half-metallic ferromagnetism
GGA + U
TB-mBJ-GGA
FP-L/APW + lo

ABSTRACT

The goal of this study is based on the determination of the half-metallic ferromagnetic features of V-doped Cu_2O alloys ($Cu_{2(1-x)}V_{2x}O$ ($x = 0$, 0.25, 0.50, 0.75 and 1)) using both GGA + U and TB-mBJ-GGA approximations (GGA: the generalized gradient approximation) within the accurate full potential linearized augmented plane wave plus local orbitals (FP-LAPW + lo) method implemented in the WIEN2k package. The structural properties are computed by using the GGA approximation in order to find the equilibrium structural parameters of each alloy, such as: lattice parameter, bulk modulus and its first-pressure derivative. The electronic properties calculated by TB-mBJ-GGA and GGA + U approximations show the complete half-metallicity of $Cu_{1.50}V_{0.50}O$, CuVO, $Cu_{0.50}V_{1.50}O$ and V_2O alloys, in fact, all the half-metallic gaps (E_{HM}) of the compete half-metals are given in this study. The magnetic properties of the studied alloys show that the majority of the total magnetic moment (M_{Tot}) comes from the V atom with small contributions from Cu atom and the interstitial zone. The $N_{0\alpha}$ and $N_{0\beta}$ exchange-splitting constants are given in order to analyze the contributions to conduction and valence bands during the exchange and splitting process. Furthermore, the hybridization between the *2p*-O and *3d*-V states (*p-d* hybridization) is the cause for the appearance of feeble magnetic moments on the non-magnetic Cu and O sites and the reduction of the atomic magnetic moment of the V atom.

Introduction

During this decade, half-metallic ferromagnetic materials played a remarkable and leading role in the manufacturing of new spintronic devices. A half-metallic material is a compound that exhibits semiconductive behavior in only one spin direction and metallic behavior in the other direction, leading 100 % spin-polarization at the Fermi level [1]. Since the Groot's prediction on the electronic structure of PtMnSb and NiMnSb half-Heusler alloys [2], much recent works on half-metallicity have been carried out in different families of magnetic materials, such as; in the double perovskite family like: robust half-metallic ferromagnet in doped double perovskite Sr_2TiCoO_6 by rare-earth elements [3], half metallic ferromagnetism, and transport properties of vacancy ordered double perovskites $Rb_2(Os/Ir)X_6$ (X = Cl and Br) for spintronic applications [4], demise of half-metallicity upon increasing of disorder in the double perovskite $Sr_{2-y}La_yFeMoO_6$ [5], and room temperature half metallic ferromagnetism due to Os/Ir(5d) in double - perovskites [6]; in the pinctides and chalcogenides doped with transition metal family [7] like: density functional theory investigation of half-metallic ferromagnetism in V-doped GaP alloys [8], first principles study of half-metallic ferromagnetism in Cr-doped CdTe [9], high Curie temperature and half-metallic ferromagnetism in Cr- and V-doped ZnSe in wurtzite phase [10] and theoretical investigation of electronic, magnetic and optical properties of ZnSe doped TM and co-doped with

* Corresponding author.
E-mail address: fatmimessaoud@yahoo.fr (M. Fatmi).

https://doi.org/10.1016/j.rinp.2024.107368
Received 30 November 2023; Received in revised form 12 January 2024; Accepted 18 January 2024
Available online 21 January 2024

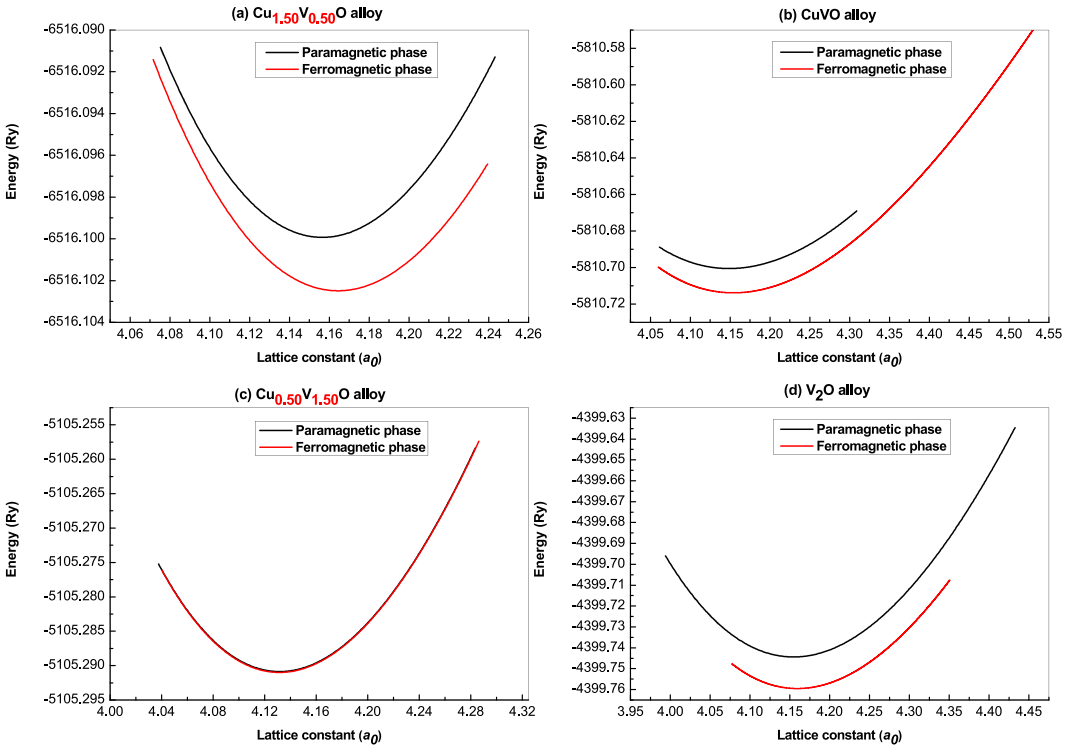

Fig. 1. Optimization of total energy versus unit-cell volume of $Cu_{2(1-x)}V_{2x}O$ alloys ((a) for $x = 0.25$, (b) for $x = 0.50$, (c) for $x = 0.75$ and (d) for $x = 1$).

Table 1
Calculated equilibrium lattice constants a_0 (in Å), bulk modulus B_0 (in GPa) and the first-pressure derivative of the bulk modulus B' of the equilibrium $Cu_{2(1-x)}V_{2x}O$ alloys ($x = 0$, 0.25, 0.50, 0.75 and 1) in paramagnetic (PM) and ferromagnetic (FM) phases, using PBE-GGA approximation.

Alloy	Phase	Lattice constant a_0 (Å)			Bulk modulus B_0 (GPa)			B'		
		This Work	Cal.	Exp.	This Work	Cal.	Exp.	This Work	Cal.	Exp.
Cu_2O	PM phase	4.308	4.2916 [a] 4.2805 [a] 4.30 [b] 4.26 [f]	4.2670 [c, d] –	112.07	– – 108 [b] 136.1 [f]	112 [e]	5.145	– – – 4.672 [f]	–
$Cu_{1.50}V_{0.50}O$	PM phase	4.1501	–	–	147.68	–	–	5.513	–	–
	FM phase	4.1579	–	–	136.24	–	–	5.359	–	–
CuVO	PM phase	4.1423	–	–	165.88	–	–	4.7623	–	–
	FM phase	4.1476	–	–	169.4	–	–	5.1148	–	–
$Cu_{0.50}V_{1.50}O$	PM phase	4.1253	–	–	190.29	–	–	4.8538	–	–
	FM phase	4.1252	–	–	191.13	–	–	4.9991	–	–
V_2O	PM phase	4.1482	–	–	197.81	–	–	3.6435	–	–
	FM phase	4.1528	–	–	192.84	–	–	4.3595	–	–

[a] Ref. [42], [b] Ref. [43], [c] Ref. [44], [d] Ref. [45], [e] Ref. [46], and [f] Ref. [47].

MnTM (TM: Fe, Cr, Co) [11]; and in the Heusler alloys family like: experimental and first-principles investigation on magnetic properties and electronic structure in half-metallic MnCoVAl Heusler alloy [12], investigation of half-metallic properties of full-Heusler alloys of O_2BaX (X = Na, K, Rb, and Cs) [13] and half metallic Heusler alloys XMnGe (X = Ti, Zr, Hf) for spin flip and thermoelectric device application [14]. Furthermore, the half-metallicity property has appeared recently in the doping of Heusler alloys [15–19].

The Cu_2O material has a semiconductive behavior with a direct band-gap about 2.17 eV [20]. It is more and more attractive in opto-electronic, photo-detection and photovoltaic applications because it has important intrinsic features and a high absorption coefficient [21–24]. The Cu_2O compound is marked by many attractive features such as: wide availability, good sensing of photon, specific stability, and non-toxicity [25]. Numerous experimental and theoretical works on the cubic compound Cu_2O are available in the literature throughout this decade, like: granular protruded irregular Cu_2O catalysts for efficient CO_2 reduction to C_2 products [26], the Cu_2O layer effect on feature properties of n-CdS/p-Cu_2O heterojunction [27], nanostructured Cu_2O deposited on TiO_2 nanotube arrays for ultra-sensitive non-enzymatic cholesterol electrochemical biosensor [28] and theoretical studies of the adsorption and dissociation of two no molecules on Cu_2O (1 1 1) surface [29]. In this approach, we studied the electronic and magnetic properties of V-doped Cu_2O alloys in order to show the half-metallic

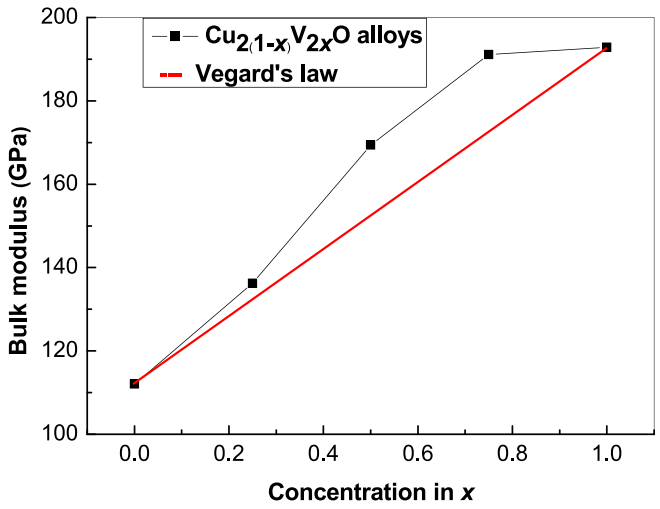

Fig. 2. Variation of equilibrium bulk modulus versus x concentration of $Cu_{2(1-x)}V_{2x}O$ alloys (x = 0, 0.25, 0.50, 0.75 and 1).

ferromagnetic character which reigns within these alloys.

This research was essentially carried out to prove the half-metallic nature of these new V-doped Cu_2O materials in order to show their wide potential use for applications in the field of spintronics (manufacture of new spintronic devices based on magnetic materials for storage of information).

The following of this article is organized as fellow: the simulation method is detailed in Section 2. Results of the structural, electronic and magnetic properties of V-doped Cu_2O alloys are given in Section 3. In the end, Section 4 brings together the main conclusions according to this approach.

Simulation detail

Within the framework of density functional theory (DFT) [30], the calculations in this study were carried out using the precise method of full-potential linearized augmented plane wave with local orbitals (FP-L/APW + lo) [31,32], which is integrated into the WIEN2*k* package [33]. The generalized gradient approximation (GGA) of Perdew–Burke–Ernzerhof [34] is selected to describe the exchange and correlation (XC) potential. The structural properties of these studied alloys are determined during this approach using the PBE-GGA approximation, while their electronic and magnetic properties are done by applying both the GGA + U (U is the Hubbard term that treats the delocalized orbitals (d and f electrons), as well as estimating the Coulomb repulsion energy) [35] and TB-mBJ-GGA (the Tran-Blaha modified Becke-Johnson potential) [36,37] approximations. The U value of vanadium atom (V) in this prediction is taken as 2.73 eV [38,39]. The radii of the muffin-tin spheres of the O, Cu, and V atoms are selected to be 1.53, 1.78, and 1.73 a.u., respectively. In this approach, to define the matrix size in order to acquire the energy eigenvalues convergence and the expansion of the plane waves, it is necessary that the $R_{MT} \times K_{Max}$ be fixed at 8; R_{MT} indicates the weakest radius of muffin-tin, whereas K_{Max} denotes the large reciprocal vector modulus, which describes expansion of the wave function. The term of Fourier expansion which translates the charge density and the expansion of the wave function is chosen to be $G_{Max} = 12$ (Ry)$^{1/2}$. The angular momentum the muffin-tin spheres is given in its largest value as $l_{Max} = 10$. The integrations in the irreducible Brillouin zone of the tetragonal $Cu_{1.50}V_{0.50}O$ and $Cu_{0.50}V_{1.50}O$ alloys were performed on the mesh of 12 × 12 × 6, where 63 special k-points are generated, while those of the cubic CuVO and V_2O alloys were carried out on the mesh of 10 × 10 × 10 which generates 35 special k-points. The valence electrons of O, Cu and V atoms are selected as: O ($2s^2 2p^4$), Cu ($3d^{10} 4s^1$) and V ($3d^3 4s^2$). Furthermore, the self-consistent iterations process continues until the total energy convergence is greater than 10^{-4} Ry.

Results and discussion

Structural properties

Crystal structure

The Cu_2O material crystallizes in the cubic structure corresponding to the space group $Pn\bar{3}m$ (no. 224) [20,25]. In this structure, O and Cu atoms are located in the following Wyckoff positions (0, 0, 0) and (¼, ¼, ¼), respectively.

For the $Cu_{2(1-x)}V_{2x}O$ system, we can distinguish two cases: for x = 0.75 and 0.25, the crystal structure becomes a tetragonal system, where the vanadium atoms are located at the following Wyckoff positions (½, 0, ¼) and (0, 0, 0), respectively; for x = 0.50, the crystal has a cubic structure, and the vanadium atoms are positioned at the (0, 0, 0) and (½,½, 0) positions.

Lattice parameters at the equilibrium

The Birch-Murnaghan's equation of state (EOS) [40,41] has been applied in this approach to proceed with the minimization of the total energy of the $Cu_{2(1-x)}V_{2x}O$ alloys at x = 0, 0.25, 0.50, 0.75 and 1, taken in ferromagnetic (FM) and paramagnetic (PM) phases. The EOS equation is given in the following relation:

$$E(V) = a + bV^{-2/3} + cV^{-4/3} + dV^{-6/3} \quad (1)$$

Where, V denotes the unit-cell volume; whereas, a, b, c and d coefficients present the fitting parameters.

The E-V curves of all $Cu_{2(1-x)}V_{2x}O$ alloys are depicted in Fig. 1. From Fig. 1, PBE-GGA calculations show that the stable ground state of $Cu_{2(1-x)}V_{2x}O$ alloys (x = 0.25, 0.50, 0.75 and 1) is reported in ferromagnetic configuration, confirming that all $Cu_{1.50}V_{0.50}O$, CuVO, $Cu_{0.50}V_{1.50}O$ and V_2O alloys are magnetic materials. The computed equilibrium lattice parameters such as: lattice constant (a_0), bulk modulus (B_0) and its first-pressure derivative (B') for the studied compounds are given in Table 1. For the case of Cu_2O compound, both calculated lattice constant and bulk modulus are in good agreement with those determined experimentally, with a deviation of 0.96 % and 0.066 %, respectively. On the other hand, the evolutions of the obtained values for bulk modulus (B_0) of the studied compounds as a function of doping concentration (x) are depicted in Fig. 2; we notice that B_0 increases with x concentration from 0 to 1; this means that the increasing concentration of V doping in the system improves its hardness.

Table 2
Calculated total energy E_0 (in Ry) of the equilibrium $Cu_{2(1-x)}V_{2x}O$ alloys (x = 0, 0.25, 0.50, 0.75 and 1) in their stable ground state, individual energies of Cu, V and O atoms (in Ry) taken in their stable phase, and the formation energy of these alloys E_f (in Ry).

Alloy	E_0	E_{Cu}	E_V	E_O	E_f
Cu_2O	−7221.467171	−3309.685737	–	−150.116889	−451.978808
$Cu_{1.50}V_{0.50}O$	−6516.102488	−3309.685737	−1898.056931	−150.116889	−452.428528
CuVO	−5810.713834	−3309.685737	−1898.056931	−150.116889	−452.854277
$Cu_{0.50}V_{1.50}O$	−5105.290989	−3309.685737	−1898.056931	−150.116889	−453.245835
V_2O	−4399.759508	–	−1898.056931	−150.116889	−453.528757

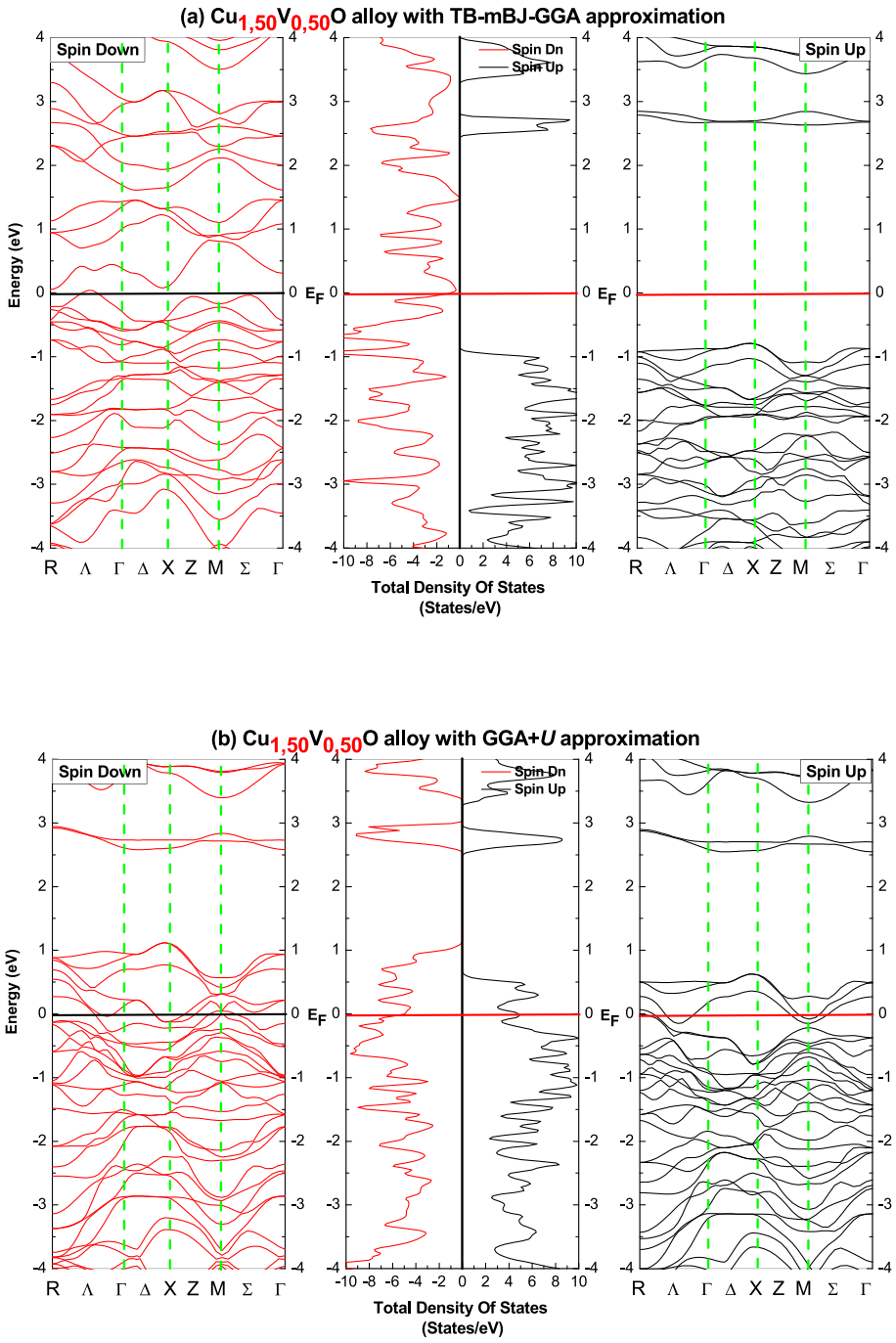

Fig. 3. Computed spin-polarized band structure and total density of states (TDOS) of the equilibrium $Cu_{1.50}V_{0.50}O$ alloy, using both (a) TB-mBJ-GGA and (b) GGA + *U* schemes.

Formation energy

Formation energy (E_f) is defined as an energy quantum necessary to keep the material stable at 0 K. When E_f is found in a negative sign, it rigorously confirms that exists a bonding connecting atoms within their favorable crystal [48]. The computed E_f of all the $Cu_{2(1-x)}V_{2x}O$ alloys at $x = 0$, 0.25, 0.50, 0.75 and 1 are found according to the following expressions [49–53]:

$$E_f(Cu_{2(1-x)}V_{2x}O) = E_0 - (4(1-x)E_{Cu} + 4xE_V + 2E_O) \quad (2)$$

E_0 denotes the total energy of each compound, and E_O, E_{Cu} and E_V are the individual energies of O, Cu and V atoms in their favorable crystal structure, respectively. The E_f values obtained for each alloy are gathered in Table 2; therefore, the calculated E_f of all the studied compounds is found with a negative sign, increasingly confirming their stability.

Electronic structure

The TB-mBJ-GGA and GGA + *U* calculations of the electronic structure of V-doped Cu_2O alloys were carried out in order to understand their electronic role in further spintronic, optoelectronic and magneto-electronic projects and also to give important information about their electronic functionalities.

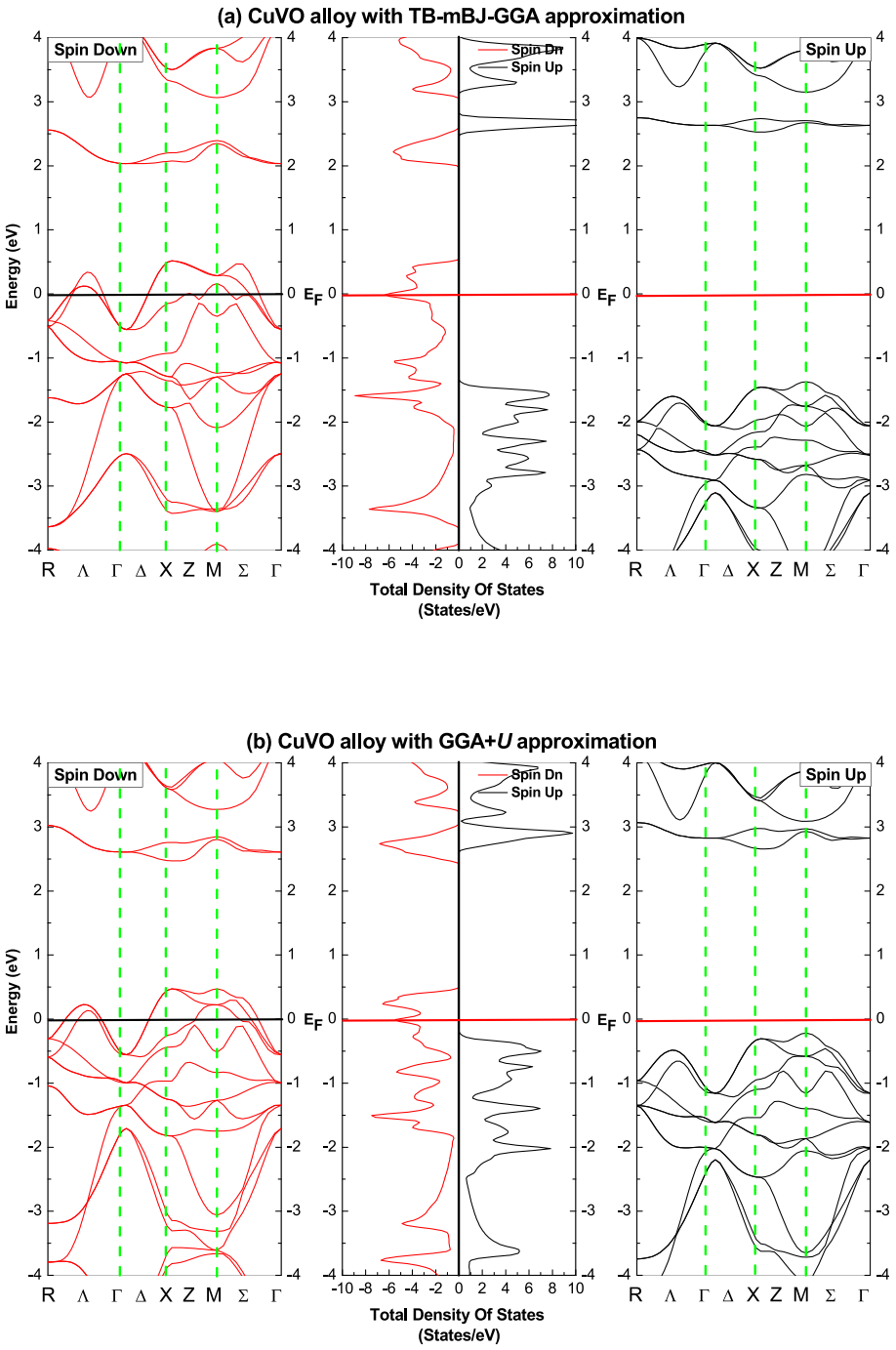

Fig. 4. Computed spin-polarized band structure and total density of states (TDOS) of the equilibrium CuVO alloy, using both (a) TB-mBJ-GGA and (b) GGA + *U* schemes.

Equilibrium spin-polarized band structure

The equilibrium spin-polarized band structures of V-doped Cu_2O alloys ($Cu_{2(1-x)}V_{2x}O$ alloys at x = 0.25, 0.50, 0.75 and 1) have been determined at the equilibrium employing both GGA + *U* and TB-mBJ-GGA settings, along the directions of high symmetry. Figs. 3-6 depict the spin-polarized total density of states and band structures of $Cu_{1.50}V_{0.50}O$, CuVO, $Cu_{0.50}V_{1.50}O$ and V_2O alloys, respectively. So, it is clear that is a large exchange and splitting between majority-spin and minority-spin states. In Figs. 3-6, majority-spin (spin-down) band structures of $Cu_{1.50}V_{0.50}O$, CuVO, $Cu_{0.50}V_{1.50}O$ and V_2O alloys exhibit a metallic behavior due to the overlap between valence and conduction bands, while their minority-spin (spin-up) band structures have a semiconductive character because the Fermi level falls within the energy gap; this means that all $Cu_{2(1-x)}V_{2x}O$ alloys (x = 0.25, 0.50, 0.75 and 1) have a complete half-metallic nature, leading to 100 % spin-polarization at the Fermi level.

The half-metallic gap (E_{HM}) is defined as the minimum between the lowest energy of the majority-spin and minority-spin conduction bands with respect to the Fermi level, and the absolute values of the highest energy majority-spin and minority-spin valence bands [54,55]. On the other hand, the half-metallic gap (E_{HM}) and minority-spin band-gap (E_g) of V-doped Cu_2O alloys are computed using GGA + *U* and TB-mBJ-GGA schemes, in fact, their computed values are listed in Table 3. Importantly, the larger half-metallic gap promises the possibility to achieve

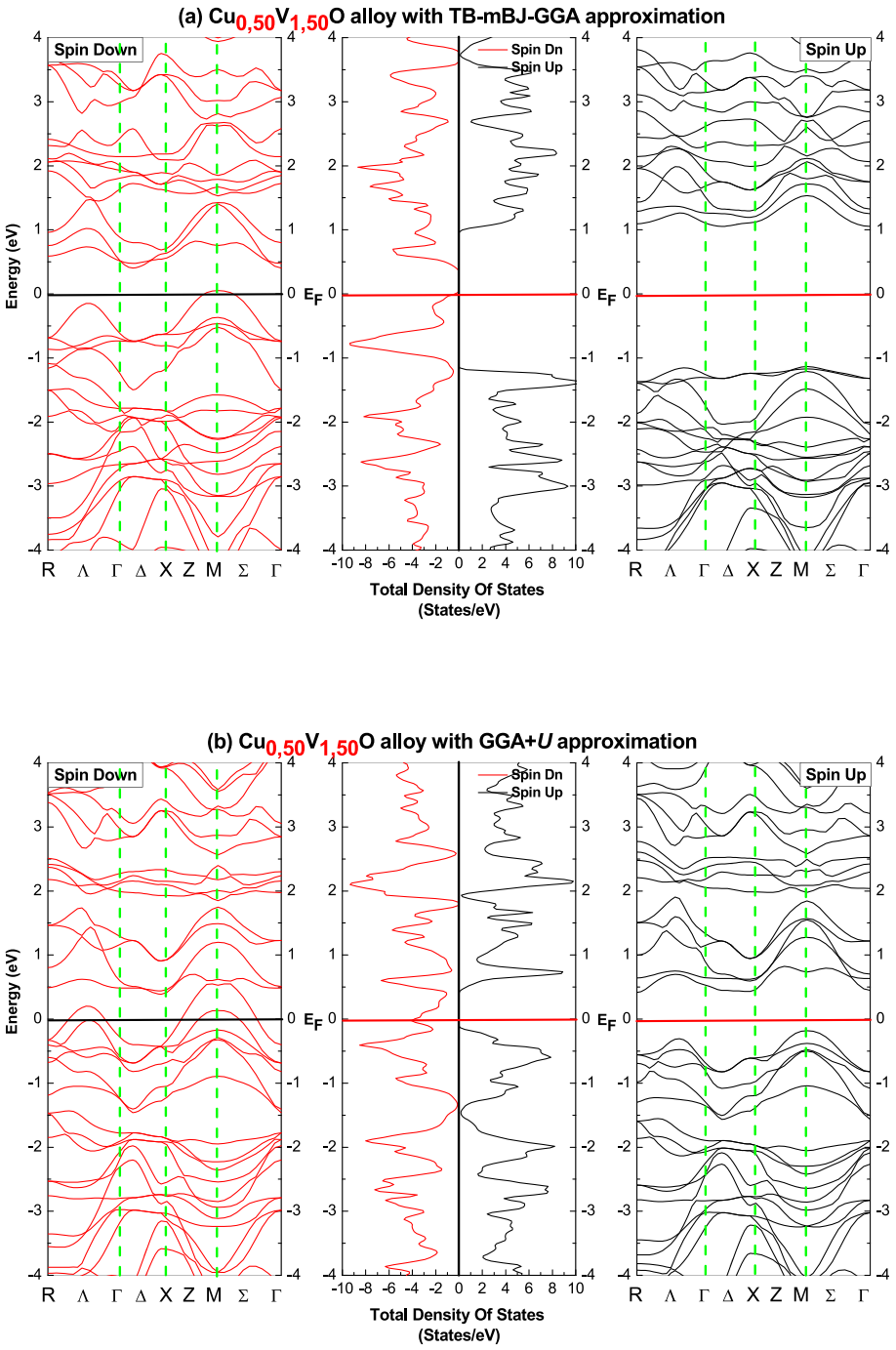

Fig. 5. Computed spin-polarized band structure and total density of states (TDOS) of the equilibrium $Cu_{0.50}V_{1.50}O$ alloy, using both (a) TB-mBJ-GGA and (b) GGA + *U* schemes.

high Curie temperature for experimental work on V-doped Cu_2O alloys. From the analysis of the results, we can deduce that the E_{HM} values of half-metallic alloys given by the TB-mBJ-GGA parameterization are improved than those calculated by the GGA + *U* approximation.

Electronic density of states

For each electronic investigation on materials, it is obligatory to go through the calculation of the electron density of states in order to describe in detail their bonds and their electronic structure, and to predict their potential application in optoelectronic, electronic and spintronic devices. In this fact, the spin-polarized partial density of states (PDOS) spectra of $Cu_{2(1-x)}V_{2x}O$ alloys ($x = 0.25$, 0.50, 0.75 and 1) were done using GGA + *U* and TB-mBJ-GGA approximations, where their curves are shown in Figs. 7–10, respectively.

For the $Cu_{1.50}V_{0.50}O$ alloy, the PDOS curves performed by both GGA + *U* and TB-mBJ-GGA approximations are mostly contributed by *3d*-V states in the energy range around the Fermi level (E_F) for spin-down panel (from −1.35 to 1.47 eV), while these states (*3d*-V state) occupy the lower part compared to E_F for the case of spin-up; thus, contributions in the energy ranges from −6.40 eV to E_F for both spin-up and spin-down case and from −7.49 eV to E_F for the spin-up and spin-down cases come from *2p*-O and *3p*-Cu states, respectively. Importantly, the *3d*-V electrons are at the origin of the half-metallic behavior of this alloy, because they occupy the region around E_F for the spin-down direction, while this

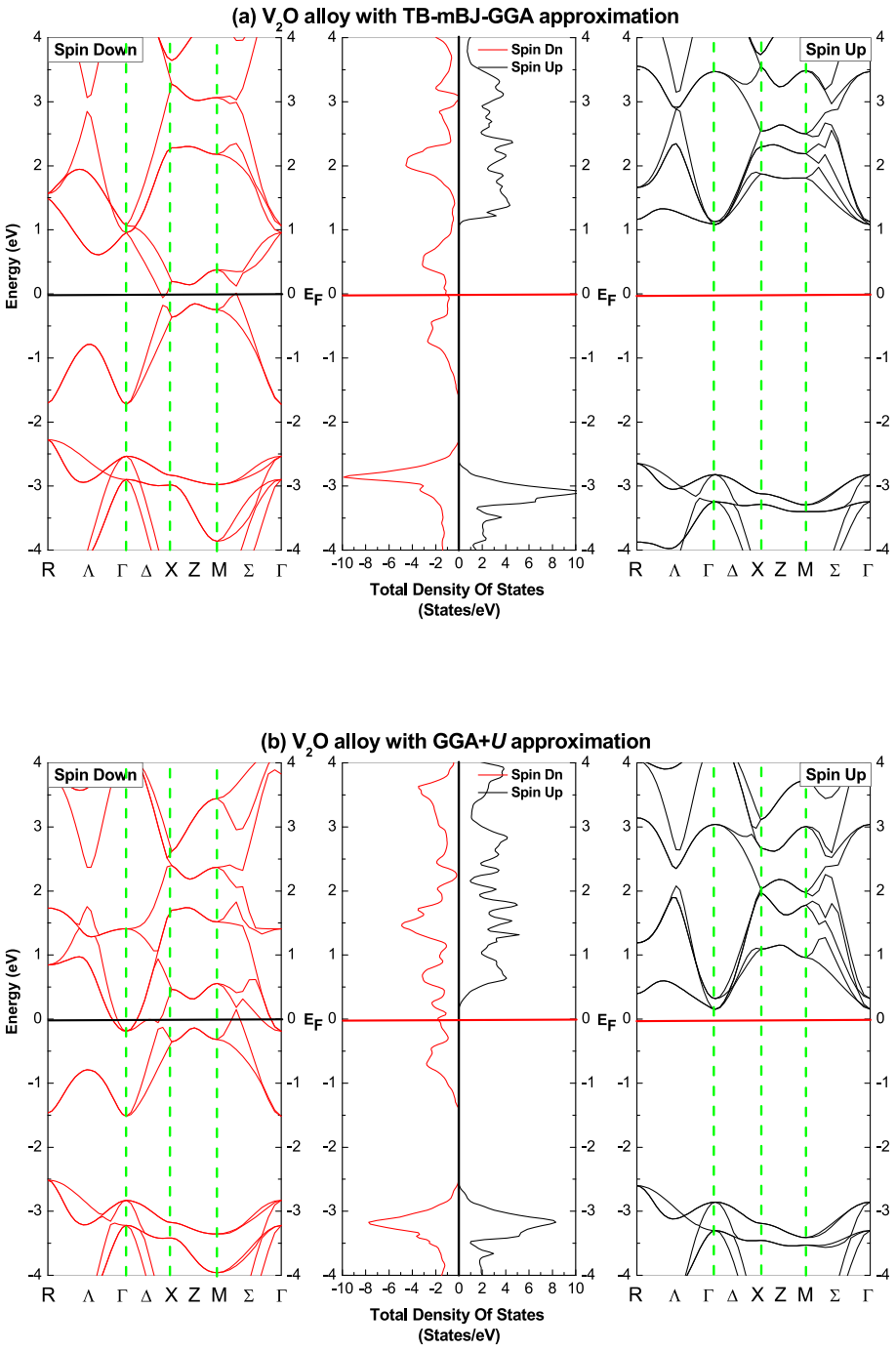

Fig. 6. Computed spin-polarized band structure and total density of states (TDOS) of the equilibrium V_2O alloy, using both TB-mBJ-GGA and GGA + *U* schemes.

region is empty of the spin-up direction.

In the case of the CuVO alloy, the *3d*-V electrons occupy the region around E_F for the majority spin case (spin-down) and the lower and upper regions relative to E_F for the minority spin case (spin-up). Moreover, the *3d*-Cu and *2p*-O states are the bands located in the spectra from −6.43 and −1.40 eV for the spin-up orientation and from –5.63 to 0.56 eV for the spin-down orientation.

In the case of the $Cu_{0.50}V_{1.50}O$ alloy, the spin-down parts around E_F and the parts below E_F for the spin-up direction are occupied by the *3d*-V electrons; the *3p*-Cu orbitals belong to the spin-down and spin-up energy region from −6.34 to −1.13 eV. Furthermore, *2p*-O states corresponding of spin-down and spin-up directions are the bands located in the energy region between −6.67 and −1.17 eV and between −6.16 eV and E_F, respectively.

It is evident that there is a strong hybridization between *3d*-V and *2p*-O states along the DOS spectrum, where this hybridization is observed in all $Cu_{1.50}V_{0.50}O$, CuVO, and $Cu_{0.50}V_{1.50}O$ and V_2O cases.

In the case of the V_2O alloy, the bands that belong of spin-up energy region from −6.30 to −2.87 eV and from 1.11 to 4.99 eV arise from *3d*-V electrons, whereas the spin-down *3d*-V electrons appear in the energy regions between −6.21 and −2.40 eV and between −1.58 and 4.97 eV, the *2p*-O states occupy the energy ranges between −6.25 and −2.60 eV and between 1.38 and 4.92 eV for the spin-up panel, while they are spotted in the energy zones between −6.25 and −2.33 eV and between −1.41 and −2.33 eV in the case of spin-down panel.

According to the V-doped Cu_2O process, the *3d*-V states involve the

Table 3
Calculated spin-down band gap energy E_g (in eV), half-metallic gap energy E_{HM} (in eV), *3d*-V band exchange splitting $\Delta_x(d)$ (in eV) and $N_{0\alpha}$ and $N_{0\beta}$ exchange constants of the equilibrium $Cu_{2(1-x)}V_{2x}O$ alloys ($x = 0$, 0.25, 0.50, 0.75 and 1), where the GGA + *U* values are between brackets.

Alloy	E_g	E_{HM}	$\Delta_x(d)$	$N_{0\alpha}$	$N_{0\beta}$
Cu_2O	0.81	–	–	–	–
$Cu_{1.50}V_{0.50}O$	3.2926	0.8523	0.6236	−6.5075 (–)	2.2728
	(–)	(–)	(0.1062)		(–)
CuVO	3.7824	1.3197	1.1143	−3.2836	1.7596
	(2.7756)	(0.1731)	(0.5341)	(−3.4700)	(0.2308)
$Cu_{0.50}V_{1.50}O$	2.0953	0.9416	0.0895	−0.8370	1.0255
	(0.4898)	(0.1064)	(0.1328)	(−0.3408)	(0.0946)
V_2O	3.6191	1.0279	0.0678	−0.6853	1.7275
	(2.6939)	(0.1476)	(0.0984)	(−0.1968)	(1.6975)

electronic structure of the Cu_2O semiconductor by bringing the energy of exchange and splitting ($\Delta_x(d)$), where, it presents the difference in energy between highest peaks of the majority and minority orientations [56]. $\Delta_x(d)$ is given as follow [56]:

$$\Delta_x(d) = E_d(\downarrow) - E_d(\uparrow) \tag{3}$$

Where,$E_d(\uparrow)$ and $E_d(\downarrow)$ present the energy of the highest peaks of the spin-up and spin-down components, respectively. Therefore, the $\Delta_x(d)$ energy of the equilibrium $Cu_{2(1-x)}V_{2x}O$ alloys is calculated using GGA + *U* and TB-mBJ-GGA approximations (see Table 3). The positive sign appearing in $\Delta_x(d)$ explains that the effective potential of the spin-up component is more and more attracted than that of the spin-down component.

Magnetic properties

Exchange-splitting constants

The $N_{0\alpha}$ and $N_{0\beta}$ exchanges-splitting constants are important parameters to describe the contributions to the conduction and valence bands during the exchange and splitting process, respectively. $N_{0\alpha}$ denotes the *s-d* exchange constant, while $N_{0\beta}$ denotes the *p-d* exchange constant, where N_0 is the concentration of the cation. The $N_{0\alpha}$ and $N_{0\beta}$ constants are expressed in the following relations according to Kondo's theory [57–59].

$$\begin{cases} N_{0\alpha} = \dfrac{\Delta E_C}{x\langle M\rangle} \\ N_{0\beta} = \dfrac{\Delta E_V}{x\langle M\rangle} \end{cases} \tag{4}$$

and

$$\begin{cases} \Delta E_C = E_C(\downarrow) - E_C(\uparrow) \\ \Delta E_V = E_V(\downarrow) - E_V(\uparrow) \end{cases} \tag{5}$$

Where, x is the transition metal concentration; $\langle M\rangle$ represents the one-half magnetization of the transition metal and ΔE_C and ΔE_V denote the edge splitting of the conduction and valence bands at Γ direction, respectively. According to the GGA + *U* and TB-mBJ-GGA parameterizations, the of $N_{0\alpha}$ and $N_{0\beta}$ computed values for the equilibrium $Cu_{2(1-x)}V_{2x}O$ alloys ($x = 0.25$, 0.50, 0.75 and 1) are reported in Table 3; in fact, $N_{0\beta}$ constant for all the full half-metallic alloys are found in positive sign, this means that the effective potential of the spin-up orientation (minority-spin states) is increasingly attracted than that of the spin-down orientation (majority-spin states). Furthermore, $N_{0\alpha}$ and $N_{0\beta}$ coupling constants of all the studied alloys are found in opposite signs, this confirms that the valence and conduction electrons interact in opposite manner during the exchange-splitting process.

Magnetic moments

In the equilibrium $Cu_{2(1-x)}V_{2x}O$ alloys at $x = 0.25$, 0.50, 0.75 and 1, the total magnetic moment (M_{Tot}), the local magnetic moments of each site of the Cu, V and O atoms and the interstitial magnetic moment in the interstitial zones are calculated using both the GGA + *U* and TB-mBJ-GGA approximations; in fact, their calculated values are reported in Table 4. We can understand from Table 4 that the main contribution of M_{Tot} of $Cu_{1.50}V_{0.50}O$, CuVO and $Cu_{0.50}V_{1.50}O$ alloys comes from the Cu atom, while the total magnetic moment of V_2O alloy is mostly contributed by the magnetic moment of the V atom. Importantly, the calculations of TB-mBJ-GGA approximation show that all alloys have a total magnetic moment in integer value, which increasingly confirms their complete half-metallic feature. The atomic magnetic moments of the V and Cu atoms in $Cu_{1.50}V_{0.50}O$, CuVO and $Cu_{0.50}V_{1.50}O$ alloys have opposite signs, this means that: the coupling is ferrimagnetic within these compounds and the valence carriers of the Cu atom interact in an anti-parallel manner with those of the V atom. Furthermore, the strong *p-d* hybridization between the *3d*-V and *2p*-O states brings local magnetic moments in the non-magnetic sites of Cu and O atoms and reduces the atomic magnetic moment of the V atom with respect to its free space charge of 3 μ_B.

Conclusions

This approach was based on the calculations of physical properties (structural, electronic and magnetic properties) of V-doped Cu_2O alloys using the FP-LAPW + lo technique within the DFT theory, where the GGA + *U* and TB-mBJ-GGA schemes were applied in these calculations in order to define the exchange and correlation potential. The main aim of this prediction is to prove the half-metallicity within these new alloys studied. The prominent conclusions from this study are summarized in the following points:

i. The structural analysis shows that the stable ground state of $Cu_{1.50}V_{0.50}O$, CuVO, $Cu_{0.50}V_{1.50}O$ and V_2O alloys is reported in ferromagnetic configuration.
ii. The formation energy of all alloys is found with a negative sign, increasingly confirming the stability of these compounds in their crystal structure.
iii. The spin-polarized electronic calculations show that all the equilibrium $Cu_{2(1-x)}V_{2x}O$ alloys at $x = 0.25$, 0.50, 0.75 and 1 are full half-metals with a large half-metallic gap.
iv. The TB-mBJ-GGA calculations are more improved than the GGA + *U* calculations because the half-metallic gaps determined by the TB-mBJ-GGA approximation are wider compared to those of the GGA + *U* approximation.
v. We found within these alloys a strong hybridization between the *2p*-O and *3d*-V states.
vi. The $\Delta_x(d)$ energy and $N_{0\beta}$ coupling constant of all alloys are found with a positive sign, this means that the effective potential of the spin-up case (minority-spin) is more attractive than of the spin-down case (majority-spin).
vii. The $N_{0\alpha}$ and $N_{0\beta}$ coupling constants are in opposite signs, confirming that the conduction and valence carriers interact antiferromagnetically during the exchange and splitting process.
viii. The total magnetic moment of the equilibrium $Cu_{2(1-x)}V_{2x}O$ alloys ($x = 0.25$, 0.50 and 0.75) is mostly due to the magnetic moment of the Cu atom.
ix. The integer value corresponding to the total magnetic moment of all equilibrium $Cu_{2(1-x)}V_{2x}O$ alloys asserts their half-metallic ferromagnetic feature.
x. The opposite signs between the local magnetic moments of the Cu and V atoms indicate that the valence band electrons of the Cu atoms interact in anti-parallel way with those of the V atom; hence, the coupling is ferrimagnetic in these alloys.

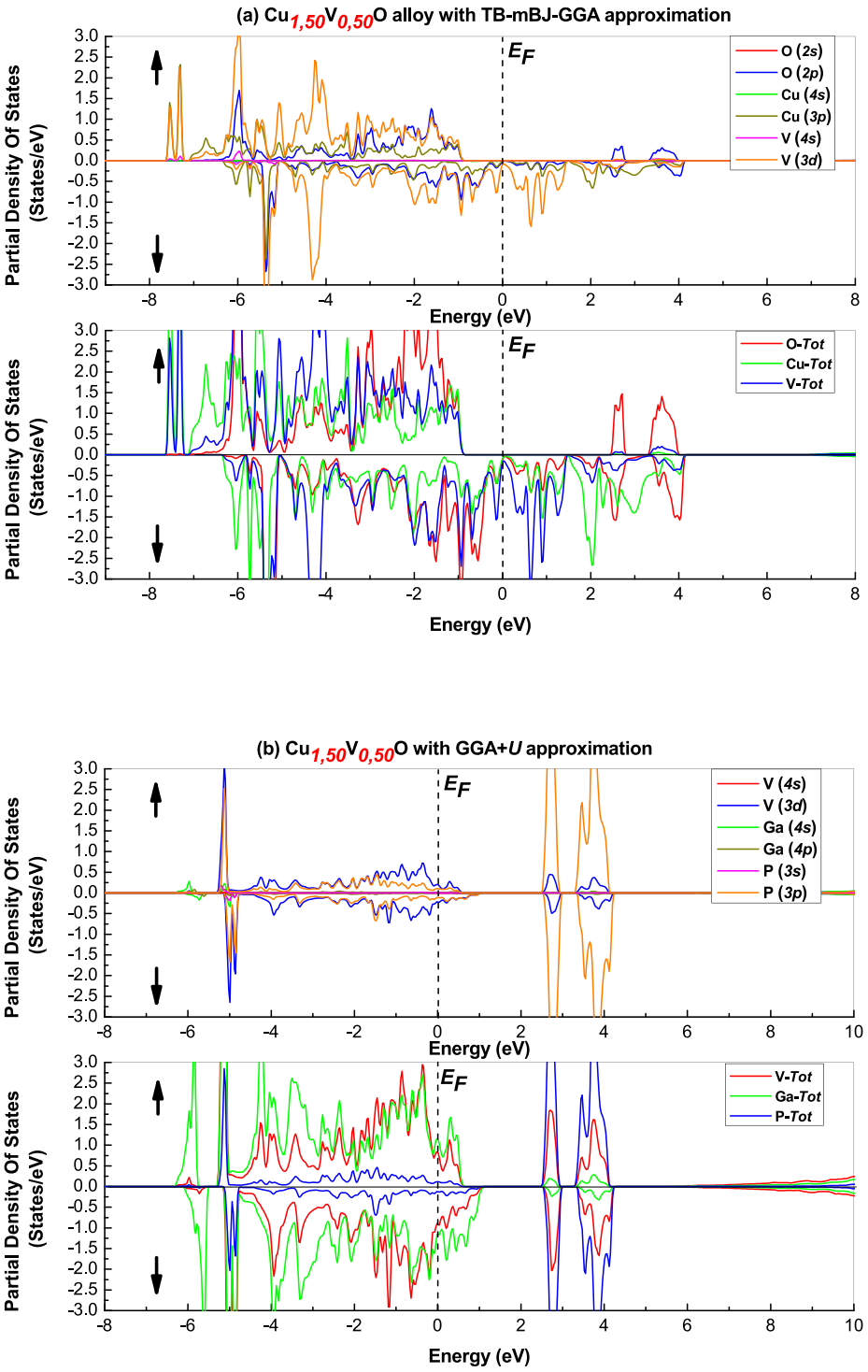

Fig. 7. Calculated spin-polarized partial density of states (PDOS) of the equilibrium $Cu_{1.50}V_{0.50}O$ alloy, using both TB-mBJ-GGA and GGA + *U* approximations.

Funding

The present work is supported by the Algerian National Scientific Research Agency's University Training Research Projects (PRFU) (Grant no. B00L02UN290120220002).

CRediT authorship contribution statement

Mohammed El Amine Monir: Conceptualization, Data curation. **Hadj Baltach:** Methodology. **Ibtisam F. Al-Maaitah:** Validation. **A.F. Al-Maaitah:** Visualization, Supervision. **M.A. Ghebouli:** Methodology, Investigation. **M. Fatmi:** Investigation. **Munirah D. Albaqami:** Software. **Saikh Mohammad:** Software. **Mika Sillanpää:** Visualization.

Declaration of competing interest

The authors declare that they have no known competing financial interests or personal relationships that could have appeared to influence the work reported in this paper.

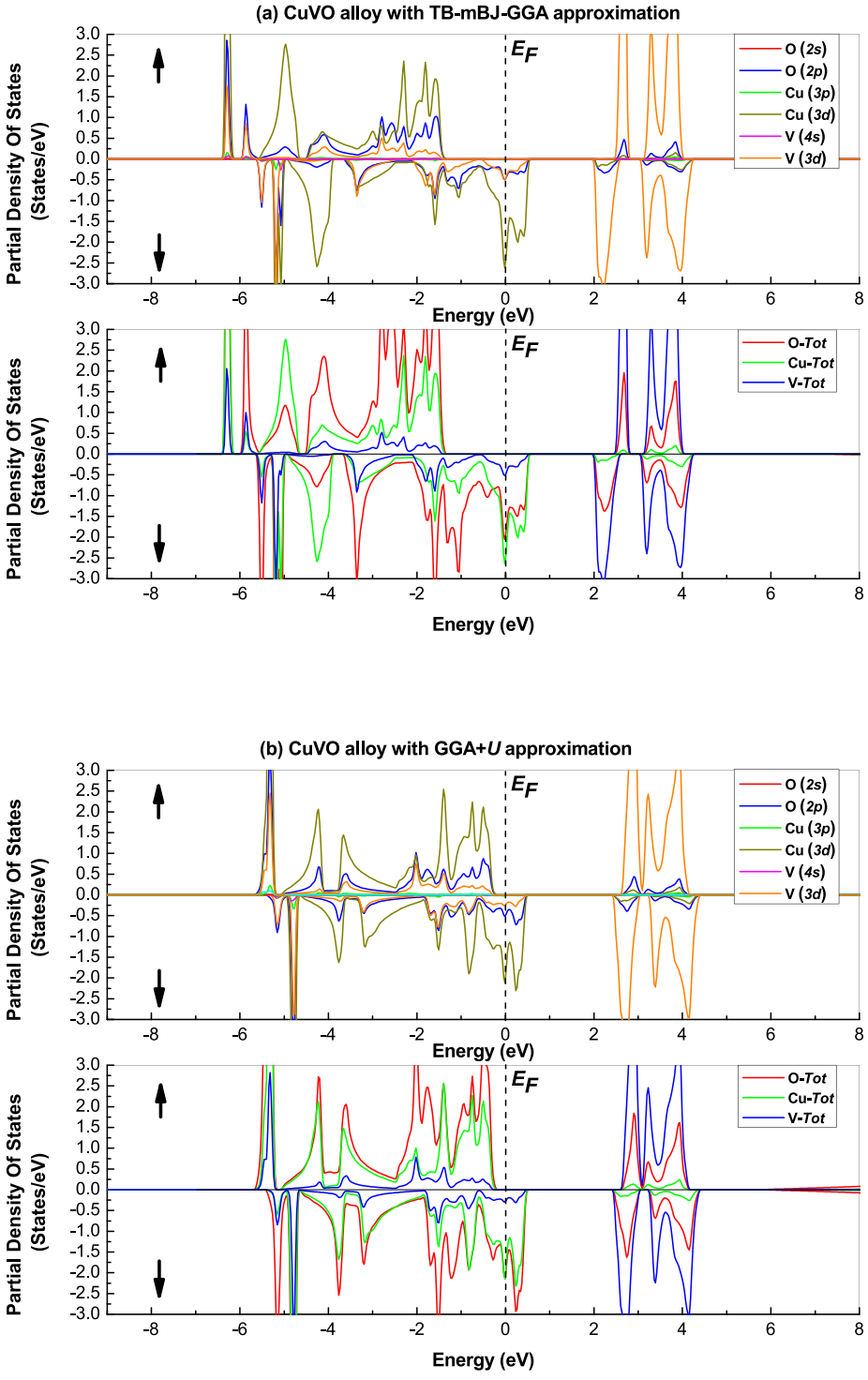

Fig. 8. Calculated spin-polarized partial density of states (PDOS) of the equilibrium CuVO alloy, using both TB-mBJ-GGA and GGA + U approximations.

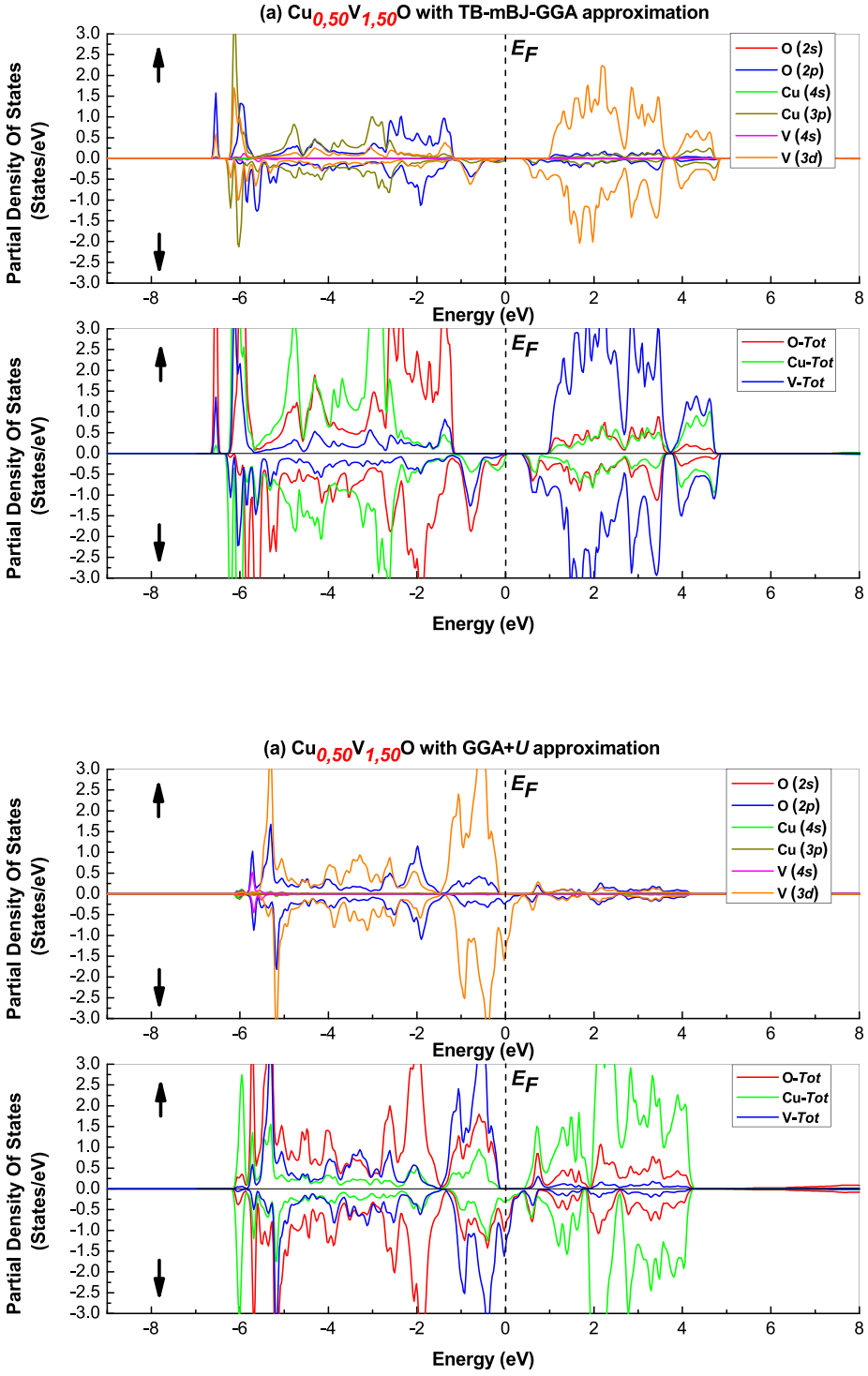

Fig. 9. Calculated spin-polarized partial density of states (PDOS) of the equilibrium $Cu_{0.50}V_{1.50}O$ alloy, using both TB-mBJ-GGA and GGA + *U* approximations.

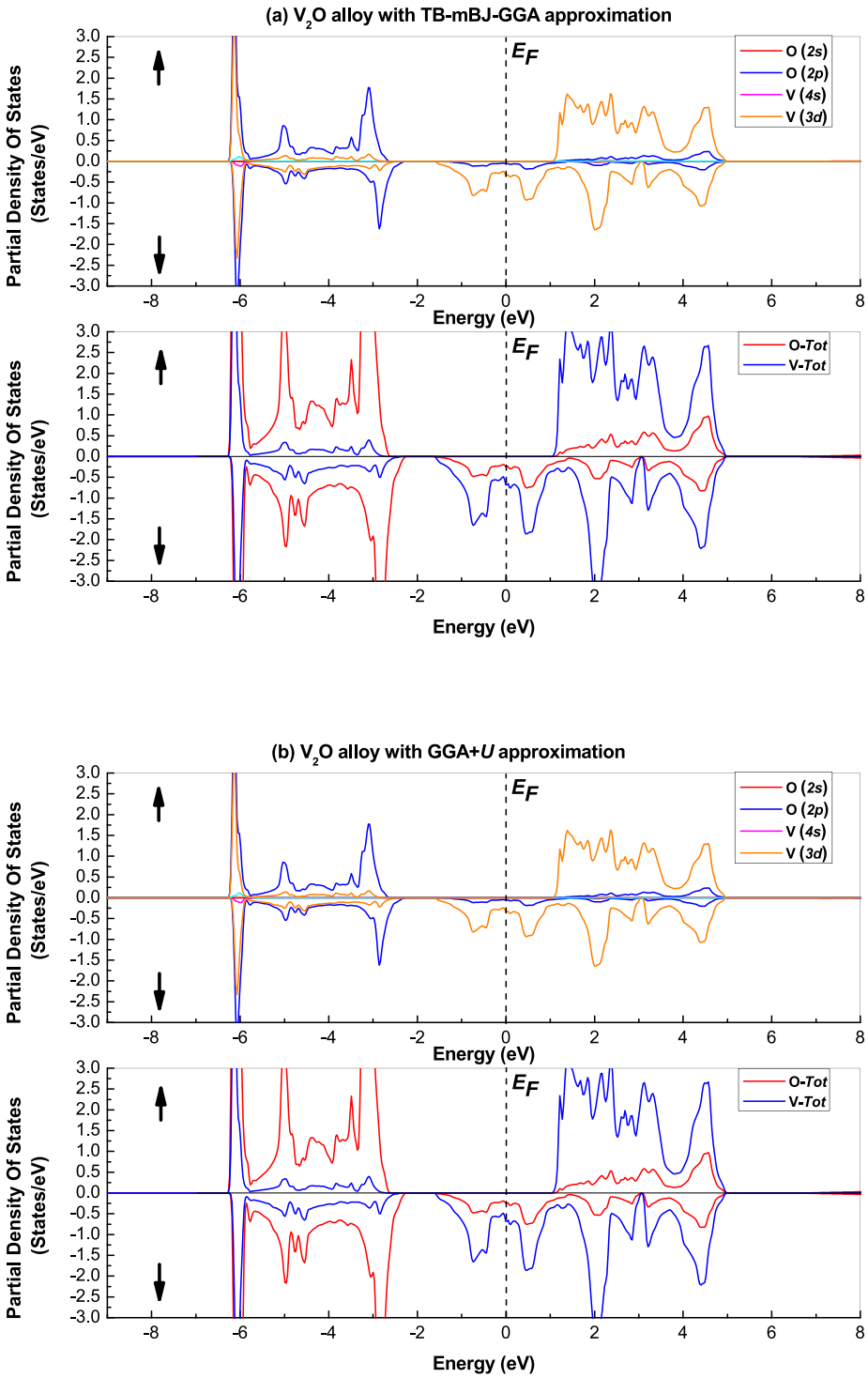

Fig. 10. Calculated spin-polarized partial density of states (PDOS) of the equilibrium V_2O alloy, using both TB-mBJ-GGA and GGA + U approximations.

Table 4
Calculated values of: the total magnetic moment M_{Tot} (in μ_B), the interstitial magnetic moment (in μ_B) in the interstitial zone and the atomic magnetic moment of each site in the equilibrium $Cu_{2(1-x)}V_{2x}O$ alloys (x = 0.25, 0.50, 0.75 and 1), where the GGA + U values are between brackets.

Alloy	Magnetic moment (μ_B)				
	M_{Tot}	Interstitial	Cu	V	O
$Cu_{1.50}V_{0.50}O$	4.00053 (3.98058)	0.13226 (0.56206)	0.98510 (0.87275)	−0.35621 (−0.26541)	0.63459 (0.53284)
CuVO	2.00007 (2.00136)	−0.20364 (0.14494)	1.04003 (0.78085)	−0.41551 (−0.13018)	0.39480 (0.30144)
$Cu_{0.50}V_{1.50}O$	0.00005 (0.00858)	0.47242 (0.21038)	0.86283 (0.24127)	−0.49940 (−0.16927)	0.08150 (0.03237)
V_2O	2.00442 (1.99729)	0.47678 (0.25240)	– (–)	0.91719 (0.85192)	−0.07668 (−0.03719)

Data availability

The data that has been used is confidential.

Acknowledgements

This work was funded by the Researchers Supporting Project Number (RSP2024R267), King Saud University, Riyadh, Saudi Arabia. The author Mohammed El Amine Monir expresses his gratitude to Professor Ángel Martín Pendás and Professor Aurora Costales of the Departamento de Química Física y Analítica, Facultad de Química, University of Oviedo, 33006-Oviedo, Spain for their assistance in this research.

References

[1] Pickett WE, Moodera JS. Phys Today 2001;54:39–44.
[2] de Groot RA, Mueller FM, van Engen PG, Buschow KHJ. Phys Rev Lett 1983;50:2024–7.
[3] Laghzaoui S, Fakhim Lamrani A, Ahl Laamara R. J Phys Chem Solid 2023;183:111639.
[4] Mustafa G-M, Hassan M, Mohammed Aloufi N, Saba S, Al-Qaisi S, Mahmood Q, et al. Ceram Int 2022;48:23460–7.
[5] Reyes AM, Montoya JA, Navarro O. J Magn Magn Mater 2020;495:165877.
[6] Mahmood Q, Nazir G, Bouzgarrou S, Rashid MS, Algrafy E, Alharthi S, et al. J Alloy Compd 2022;896:163130.
[7] Nakao M. Phys Rev B 2004;69:214429.
[8] El Amine Monir M, Bahnes A, Boukortt A, Bendoukha A, Reguig, Mouchaal Y. J Magn Magn Mater 2020;497:166067.
[9] Noor NA, Ali S, Shaukat A. J Phys Chem Solid 2011;72:836–41.
[10] Jafarova VN. Solid State Commun 2023;369:115197.
[11] Behloul M, Salmani E, Ez-Zahraouy H, Benyoussef A. J Magn Magn Mater 2016;419:233–9.
[12] Zhang Z, Wang G, Liu Y, Chen M, Xiong R, Zuo C, et al. J Alloy Compd 2023;967:171643.
[13] Nazemi N, Ahmadian F, Boochani A. Chem Phys Lett 2023;830:140751.
[14] Priyanka DS, Venkatesh G, Srinivasan M, Palanisamy G, Ramasamy P. Mater Sci Semicond Process 2023;159:107367.
[15] Rached Y, Rached D, Rached H, Cheref O, Caid M, Merabet M, et al. Eur Phys J plus 2023;138:307.
[16] Youcef A, Bettahar N, Cheref O, Benalia SE, Rached D, Benkhettou N, Bezzerga D. Rev Mex Fís 2023;69:020501.
[17] Benkaddour A, Cheref O, Benkhettou N, Mehtougui N, Rached D, Benkaddour I, et al. SPIN 2020;10:2050019.
[18] Zami F, Djoudi L, Merabet M, Benalia S, Boucharef M, Belacel R, et al. Optik 2019;180:873–83.
[19] Khirat M, Lazab M, Bettahar N, Rached D. Solid State Commun 2018;276:14–8.
[20] Kloppel A, Kriegseis W, Meyer BK, Scharmann A, Daube C, Stollenwerk J, et al. Thin Solid Films 2000;365:139.
[21] Lee S, Lee W-Y, Jang B, Kim T, Bae J-H, Cho K, et al. Device Lett 2018;39:47.
[22] Wang Y, Lany S, Ghanbaja J, Fagot-Revurat Y, Chen YP, Soldera F, et al. Phys Rev B 2016;94:245418.
[23] Yu G, Hu X, Liu D, Sun D, Li J, Zhang H, et al. J Electroanal Chem 2010;638:225.
[24] Ahmed A, Gajbhiye NS. J Solid State Chem 2010;183:3100.
[25] Hsu Y-K, Wu J-R, Chen M-H, Chen Y-C, Lin Y-G. Appl Surf Sci 2015;354:8.
[26] Jian Z, Yu J, Madatta IJ, Liu Y, Ding J. J Colloid Interface Sci 2024;653:1415–22.
[27] Güneri E, Göde F, Arı M, Saatçi B. J Mol Struct 2021;1241:130679.
[28] Kumar B, Sinha SK. Mater Today Commun 2023;37:107171.
[29] Sun B, Chen W, Xu X. Acta Phys Chim Sin 2006;22:1126–31.
[30] Hohenberg P, Kohn W. Phys Rev 1964;136:B864.
[31] Wong KM, Alay-e-Abbas SM, Shaukat A, Fang Y, Lei Y. J Appl Phys 2013;113:014304.
[32] Wong KM, Alay-e-Abbas SM, Fang Y, Shaukat A, Lei Y. J Appl Phys 2013;114:034901.
[33] Blaha P, Schwarz K, Sorantin P, Trickey SK. Comput Phys Commun 1990;59:339.
[34] Perdew JP, Burke S, Ernzerhof M. Phys Rev Lett 1996;77:3865–8.
[35] Anisimov VI, Solovyev IV, Korotin MA, Czyzyk MT, Sawatzky GA. Phys Rev B 1993;48:16929.
[36] Tran F, Blaha P. J Phys Rev Lett 2009;102:226401–4.
[37] Koller D, Tran F, Blaha P. J Phys Rev B 2011;83:195134–44.
[38] El Amine Monir M, Baltache H, Murtaza G, Khenata R, Ahmed WK, Bouhemadou A, et al. J Magn Magn Mater 2015;374:50–60.
[39] J. Kaczkowski, A. Jezierski, Institute of Molecular Physics, Polish Academy of Sciences, M. Smoluchowskiego 17 (2009) 60-179 Poznan, Poland.
[40] Murnaghan FD. Proc Natl Acad Sci 1944;30:244–7.
[41] Shang SL, Wang Y, Kim D, Liu Z-K. Comput Mater Sci 2010;47:1040–8.
[42] Ait Hssi A, Atourki L, Labchir N, Abouabassi K, Oua M, Mouhib H, et al. Mater Today Proc 2020;22:89.
[43] Ruiz AM, Moreno MG, Takeuchi N. Solid State Sci 2003;5:291.
[44] Wickoff WG. Crystal Structures, Vol. 1. New York: Wiley-Interscience; 1960.
[45] Werner A, Hocheimer HD. Phys Rev B 1982;25:5929.
[46] Beg MM, Shapiro SM. Phys Rev B 1976;13:1728.
[47] Dash LK, Bruneval F, Trinite V, Vast N, Reining L. Comput Mater Sci 2007;38:482.
[48] Yakoubi A, Baraka O, Bouhafs B. Results Phys 2012;2:58–65.
[49] Zeng ZH, Calle-Vallejo F, Mogensen MB, Rossmeisl J. Phys Chem Chem Phys 2013;15:7526–33.
[50] Rai DP, Shankar, Sandeep A, Ghimire MP, Khenata R, Thapa RK. RSC Adv 2015;5:95353–9.
[51] Bentouaf A, Naceur Y, Rached H, El Amine Belhadj M, Aissa B. Emergent Mater 2022;5:1819–30.
[52] Ould Moussa M, Kouidri S, Rached H, Haid S, Beloufa N, Ouadha I, et al. Phys A 2022;128:231.
[53] Tagrerout A, Rached H, Drief M, Guermit Y, Al-Qaisi S, Caid M, et al. Comput Condens Matter 2022;31:e00670.
[54] Yao KL, Gao GY, Liu ZL, Zhu L. Solid State Commun 2005;133:301–4.
[55] Gao GY, Yao KL, Sasioglu E, Sandratskii LM, Liu ZL, Jiang JL. Phys Rev B 2007;75:174442.
[56] Zunger A. Solid State Phys: Condensed Matter 1986;39:275.
[57] Sanvito S, Ordejon P, Hill NA. Phys Rev B 2001;63:165206.
[58] Larson BE, Hass KC, Ehrenreich H. Phys Rev B 1988;37:4137.
[59] Gaj JA, Planel R, Fishman G. Solid State Commun 1979;29:435–8.